Indonesian Journal of Science & Technology

Journal homepage: http://ejournal.upi.edu/index.php/ijost/

# Experimental and Design-Oriented Investigation of Rectangular Concrete Columns: Leveraging Low-Cost Steel Clamps and Waste Aggregates

*Phromphat Thansirichaisree [1] , Ali Ejaz[2], Hisham Mohamad[3], Preeda Chaimahawan[4,*], Saharat Buddhawanna[5], Qudeer Hussain[6]*

[1]Faculty of Engineering, Thammasat School of Engineering, Thammasat University Rangsit, Pathumthani, Thailand

[2]National Institute of Transportation, National University of Sciences and Technology (NUST), Islamabad, Pakistan

[3]Civil & Environmental Engineering Department, cc, Seri Iskandar, Malaysia

[4]School of Engineering, University of Phayao, Phayao, Thailand

[5]Civil Engineering Department, Kasem Bundit University, Thailand

[6] Faculty of Engineering, Thammasat School of Engineering, Thammasat University Rangsit, Pathumthani, Thailand

*Correspondence: E-mail: preeda.ch@up.ac.th

## ABSTRACT

Steel clamps provide a low-cost method for strengthening concrete, but their role in confining rectangular specimens remains underexplored. This study performed monotonic compression tests on rectangular specimens confined with steel clamps, examining unconfined compressive strength, number of clamps, and coarse aggregate type, including recycled brick aggregates. All specimens showed two-phase stress–strain behavior, with significant strength and ductility gains from passive confinement. Strength improved up to 91.19%, while peak strain increased by 150%, especially in specimens using recycled brick aggregates from higher-strength bricks (CB1). CB1-based concrete exhibited the greatest enhancement. Confinement ratio strongly affected efficiency. Analytical models predicting peak strength, peak strain, and post-peak modulus achieved high accuracy ($R^2$ > 0.85).

## ARTICLE INFO

***Article History:***
*Submitted/Received 24 May 2025*
*First Revised 20 Jun 2025*
*Accepted 24 Aug 2025*
*First Available Online 29 Aug 2025*
*Publication Date 01 Sep 2026*

***Keyword:***
*Analytical modeling,*
*Concrete,*
*Confinement,*
*Rectangular columns,*
*Regression,*
*Steel clamps.*

## 1. INTRODUCTION

Managing the waste generated from demolished structures remains a significant environmental challenge. A sustainable and durable solution is essential to minimize the ecological impact of this debris. In recent years, researchers have investigated the potential of incorporating demolition waste as a partial substitution for natural coarse [1–3] or fine aggregates [4–6] in concrete production, resulting in what is commonly referred to as Recycled Aggregate Concrete (RAC). Utilizing such waste helps mitigate its environmental impact [7] while also conserving rapidly depleting natural aggregate sources [8]. Currently, global concrete consumption is estimated at around 30 million tons annually [9]. Forecasts suggest this demand could rise to approximately 18 billion tons per year by 2050 [10], with an average consumption of three tons per person each year [11]. RAC offers a promising approach to reduce reliance on finite natural stone resources [12]. Research has demonstrated that substituting half of the amount of natural aggregates using recycled brick aggregates (RBA) may lower carbon releases by up to 30% and decrease landfill usage by around 40% [13,14]. Additionally, concrete made with RBA can attain compressive strengths ranging from 25 to 40 MPa, indicating its viability for structural use [15].

Extensive research on RAC has been carried out and is largely regarded as comprehensive and mature [12]. This is evidenced by the development of formal standards such as GB/T25177–2011, which pertains to recycled coarse aggregates, and GB/T25176–2011, which addresses recycled fine aggregates for use in concrete and mortar. As a result, current research trends have shifted toward exploring alternative types of construction and demolition waste, including brick [16], ceramic [17], rubber [18], and glass materials [19]. Recent investigations highlight a consistent and rapid annual increase in brick waste generation [20,21]. In the United States alone, environmental reports from 2012 to 2014 revealed that roughly 44 million tons of brick waste were produced from construction and demolition works [22]. This significant quantity emphasizes the urgent necessity for effective brick waste recycling strategies to decrease dependency on landfilling. The negative effect of RBA on concrete characteristics is generally more significant than the benefits they offer [23,24]. The crushing value of RBA ranges between 20% and 40%, indicating that these aggregates can withstand moderate compressive stress before failure [25]. RBAs exhibit higher apparent density, water absorption, and crushing index related to natural coarse aggregates [26]. Furthermore, RBA typically have a less uniform particle size distribution and often include a wider range of sizes. This heterogeneity stems from the brick production procedure, which yields particles of varying shapes and dimensions. On the contrary, natural aggregates tend to have greater uniform size distributions, shaped largely by their geological formation processes [27].

The density of recycled brick aggregate concrete (RBAC) is generally lesser than that of concrete made with natural aggregates [28]. This lower density contributes to RBAC's enhanced water absorption capacity [29]. Additionally, the elastic modulus of RBAC tends to decrease as the replacement level of brick aggregates increases [30,31]. The mechanical properties of RBAC are often significantly inferior to those of natural aggregate concrete [32,33]. For example, a reduction of approximately 40% in compressive strength and 50% in elastic modulus when comparing RBAC to natural aggregate concrete [34]. Replacement ratios below 15%, the reduction in compressive strength was minimal; however, when the replacement surpassed 30%, strength reductions surpassed 20% [35]. A full replacement of natural aggregates with RBA and observed a complete slump loss after 165 minutes in concrete made with oven-dried brick aggregates, whereas this issue was not present when

DOI: https://doi.org/10.17509/ijost.v11i2.89779
p- ISSN 2528-1410 e- ISSN 2527-8045

using saturated surface dry aggregates [36]. Improvement in porosity of up to 10% in RBAC compared to conventional concrete. Larger mean particle sizes of brick aggregates negatively impacted the tensile strength of RBAC [37]. Nonetheless, some studies have indicated that the failure modes of RBAC are comparable to those of natural aggregate concrete [38]. The primary drawbacks of RBAC are ascribed to the higher water absorption of brick aggregates, which is a result of their inherently porous structure [39]. On the positive side, RBAC offers advantages such as reduced weight relative to natural aggregate concrete, due to the higher porosity of the aggregates, and improved fire resistance, owing to the natural refractory properties of brick materials [39]. Several strategies have been implemented to improve the performance of RBAC. These comprise physical modification [40] or chemical surface treatments [41] of brick aggregates, mix design optimization [34,42] incorporation of fibers into the concrete matrix [43,44], and external confinement using various jacketing techniques [45–47]. Microbially brought carbonate precipitation (MICP) improved the quality of RBA and improved the mechanical performance of the concrete [48]. Furthermore, enzyme-induced carbonate precipitation (EICP) provided even better results by ensuring a more uniform distribution of $CaCO_3$ precipitation. Extending the incubation period in MICP treatment led to a significant decrease in the water absorption capacity of brick aggregates, addressing a major drawback [49]. a cost-effective and environmentally friendly artificial reef concrete utilizing 100% recycled brick-concrete aggregate. A comparative analysis showed that using recycled aggregates in combination with industrial by-products like fly ash and silica fume decreased carbon releases and construction expenses by up to 64%, while maintaining equivalent performance to natural aggregate alternatives [50].

Fiber-Reinforced Polymer (FRP) sheets are commonly employed in strengthening applications. The effectiveness of FRP sheets in enhancing the compressive behavior of RBAC has been investigated by several studies. Gao et al. [47] observed significant improvements in both peak compressive strength and corresponding strain of RBAC when confined with Glass FRP (GFRP) or Carbon FRP (CFRP). Jiang et al. [46] found that up to a 30% substitution of natural aggregates with brick aggregates did not adversely affect the mechanical performance of RBAC. However, further increases in the replacement ratio beyond 30% led to reductions in both elastic modulus and peak compressive stress. Although FRP confinement effectively enhances the structural performance of RBAC, the high cost associated with these materials presents a major limitation in rehabilitation projects [51,52]. For instance, CFRP, while offering excellent performance, can cost around 150 USD per square meter per layer [55]. Therefore, identifying economical and efficient alternatives to FRP confinement is essential to achieving cost-effective yet structurally sound solutions. Steel spiral confinement to improve the mechanical properties of recycled concrete. Their findings indicated that while the elastic modulus decreased with increased confinement, both confined strength and corresponding strain experienced significant enhancement [53]. A cost-effective external confinement method using standard steel hose clamps to enhance the compressive behavior of RBAC of circular cross-section [54]. They tested circular concrete cylinders with two target strength levels and applied 3, 5, and 11 steel clamps. The confinement offered by steel clamps substantially improved the confined strength and altered the failure pattern of RBAC, yielding better response than that of concrete made with natural aggregates. Recently, steel clamps to strengthen the compressive response of square-shaped concrete made with natural or RBA. Also, proposed a uniform model by combining the specimens tested by their study [55] and [56].

Previous investigations by [54] and [55] established the efficacy of steel clamp confinement in enhancing the compressive performance of RBAC. However, these studies were restricted

DOI: https://doi.org/10.17509/ijost.v11i2.89779
p- ISSN 2528-1410 e- ISSN 2527-8045

to specimens with circular or square cross-sections. It is well established that confinement effectiveness diminishes when the cross-sectional geometry transitions from circular to square, or from square to rectangular. Therefore, evaluating the performance of steel clamps on rectangular specimens is essential. This study includes an experimental program involving monotonic compression tests. Key variables examined include the unstrengthened compressive strength of concrete, the quantity of steel clamps, and the kind of coarse aggregates used.

## 2. METHODS

### 2.1. Summary of Rectangular Specimens

**Table 1** presents the test samples along with their respective group classifications. Two primary groups were defined depending on the kind of brick aggregates: G1 and G2 included recycled brick aggregates identified as CB1 and CB2, respectively. CB1 aggregates originated from cement-clay interlocking bricks, while CB2 came from demolished cement-clay interlocking brick walls. In both cases, 50% of natural coarse aggregates in the concrete mix were replaced with recycled brick aggregates. Each group was further split into two subgroups based on target compressive strength—15 MPa (Type-A) and 25 MPa (Type-B). Every subgroup consisted of four specimen types: an unconfined control specimen and 3 specimens confined with 3, 5, or 11 steel clamps. The specimen ID system included three components: concrete strength type, aggregate type, and clamp configuration. For example, B-CB2-11CL refers to a Type-B specimen using CB2 aggregates and confined with 11 clamps. **Figure 1** graphically illustrates the naming convention. Two alike samples were tested for each formation, following methodologies from prior studies [56-59]. **Figure 2(a)** shows the cross-section details, while **Figure 2(b)** shows the clamp layout. A minimum corner radius of 13 mm was used to reduce stress concentrations, in line with ACI 440 guidelines.

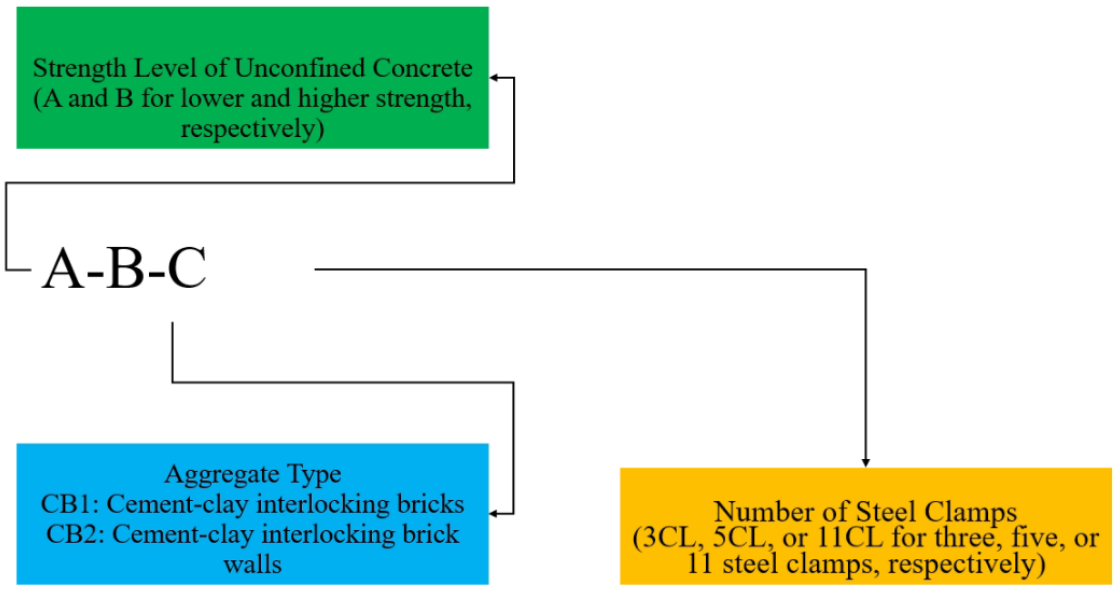


**Figure 1.** Implemented terminology for samples in this study.

DOI: https://doi.org/10.17509/ijost.v11i2.89779
p- ISSN 2528-1410 e- ISSN 2527-8045

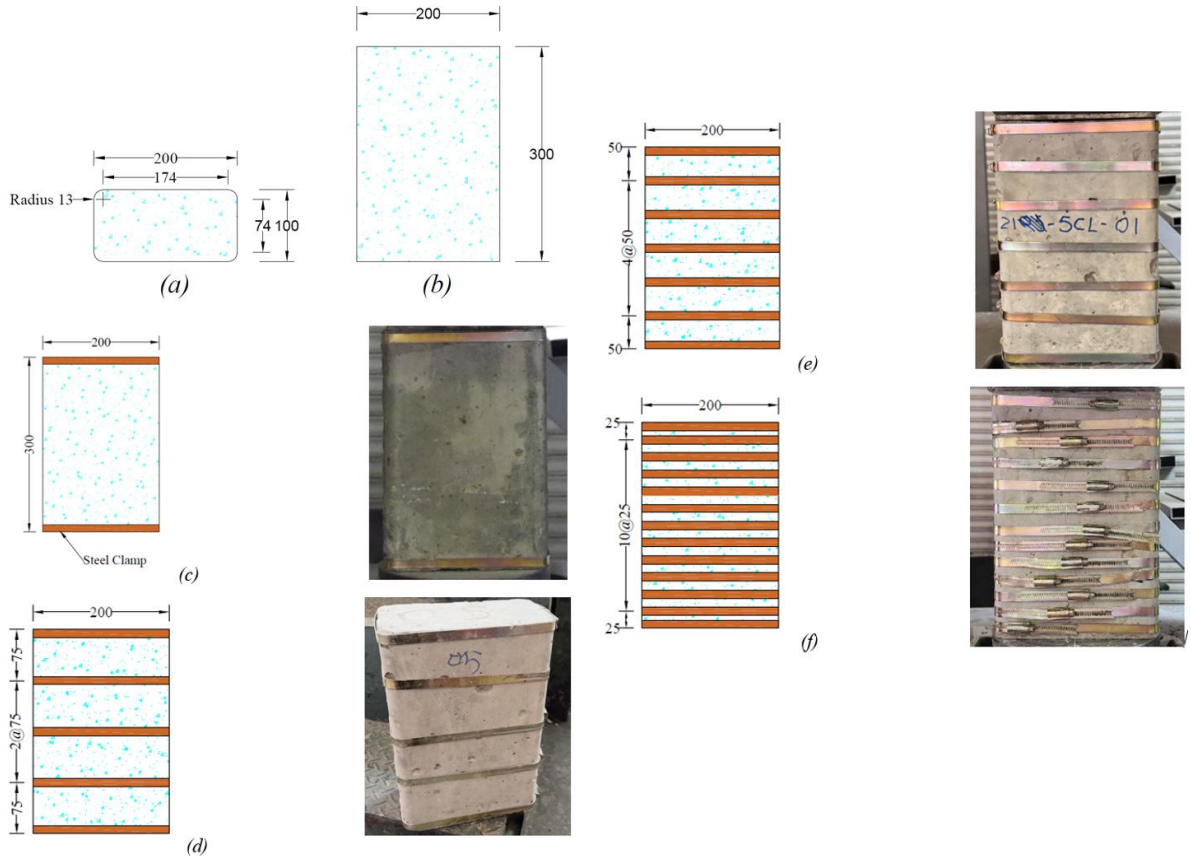


**Figure 2.** (a) sectional details, (b) front elevation, (c) control, (d) 3CL, (e) 5CL and (f) 11CL (Dimensions are presented in units of mm).

## 2.2. Properties of Materials

Recycled brick aggregates (**Figure 3**) were sourced from cement-clay interlocking and demolished cement-clay interlocking brick walls, with their properties evaluated following standard procedures and summarized in **Table 2**. To determine water absorption, 5 brick specimens were oven-dried at 110 °C for one day, chilled to ambient temperature, and weighed in their dry state. The bricks were then immersed in water for another day, surface-dried using a damp cloth, and weighed again to determine their saturated surface-dry mass. Water absorption was calculated based on the difference between dry and saturated weights. Portland cement Type I served as the binding material, while natural river sand was employed as fine aggregate. The concrete mixes were designed to achieve target slump values of 75 mm for Type-B and 85 mm for Type-A mixes, respectively. The mix proportions are provided in **Table 3**. Coarse aggregates used in the mixes ranged in size from 9.5 mm to 19.5 mm. The tensile stress vs. strain behavior of the steel clamps (**Figure 4**) was evaluated following the ASTM E8 standard, as shown in **Figure 5**. Each clamp had a width of 9 mm and a thickness of 1.1 mm. **Figure 3** presents the typical geometry and appearance of the steel clamps used in this study. These clamps were chosen for their ease of application, as they can be installed without specialized equipment. The failure pattern observed during testing is depicted in **Figure 3(c)**. To ensure accuracy and realistically simulate the confinement process, the fastener was employed inside the gage length of the specimen. Fracture consistently occurred outside the fastener zone, and the resulting tensile stress–strain curve (**Figure 3(b)**) demonstrated a ductile behavior of the steel clamps.

DOI: https://doi.org/10.17509/ijost.v11i2.89779
p- ISSN 2528-1410 e- ISSN 2527-8045

**Table 1.** Summary of rectangular specimens used in this study.

| Group | Subgroup | Specimen ID | Coarse Aggregate | Concrete Type | Number of Clamps |
|---|---|---|---|---|---|
| G1 | G1A | A-CB1-CON | NCS+CB1 | A | 0 |
| | | A-CB1-3CL | NCS+CB1 | A | 3 |
| | | A-CB1-5CL | NCS+CB1 | A | 5 |
| | | A-CB1-11CL | NCS+CB1 | A | 11 |
| | G1B | B-CB1-CON | NCS+CB1 | B | 0 |
| | | B-CB1-3CL | NCS+CB1 | B | 3 |
| | | B-CB1-5CL | NCS+CB1 | B | 5 |
| | | B-CB1-11CL | NCS+CB1 | B | 11 |
| G2 | G2A | A-CB2-CON | NCS+CB2 | A | 0 |
| | | A-CB2-3CL | NCS+CB2 | A | 3 |
| | | A-CB2-5CL | NCS+CB2 | A | 5 |
| | | A-CB2-11CL | NCS+CB2 | A | 11 |
| | G2B | B-CB2-CON | NCS+CB2 | B | 0 |
| | | B-CB2-3CL | NCS+CB2 | B | 3 |
| | | B-CB2-5CL | NCS+CB2 | B | 5 |
| | | B-CB2-11CL | NCS+CB2 | B | 11 |

Note: NCS refers to Natural Crushed Stone; CB1 and CB2 denote coarse aggregates sourced from cement-clay interlocking and clay burnt, respectively.

**Table 2.** Mechanical characteristics of bricks.

| Aggregate type | Density (kg/m3) | Compressive Strength (MPa) | Water Absorption (%) |
|---|---|---|---|
| CB1 | 130 | 6.30 | 12.30 |
| CB2 | 180 | 5.04 | 13.58 |

**Table 3.** Mix design of Type-A and Type-B concrete.

| Concrete Type | Ingredients $(\mathbf{kg/m^3})$ | | | | |
|---|---|---|---|---|---|
| | Cement | Sand | NCS | Brick Aggregates | Water |
| A | 275 | 785 | 560 | 520 | 310 |
| B | 650 | 825 | 360 | 355 | 255 |

### 2.3. Specimen Preparation

Locally available recycled bricks were first crushed into smaller fragments using a mechanical crusher. Sieve analysis was then performed on the crushed material to obtain recycled brick aggregates within the required size range, with a maximum size limit of 25 mm for all coarse aggregates. Concrete specimens were cast using steel molds. Following the guidelines of ASTM C943, concrete was placed in three equal layers, with each layer compacted using a vibration table to ensure proper consolidation (**Figure 6**). After 24 hours of casting, the specimens were demolded and subjected to a curing period of 28 days. The strengthening procedure was initiated after the concrete specimens had undergone 28 days of curing. Steel clamps were installed in their designated positions and secured by tightening screws. A torque wrench was used to ensure consistent tightening across all specimens. In accordance with previous studies [54,55], each clamp was tightened with a uniform torque of 5 N·mm to ensure standardized confinement conditions. Typical low-cost steel clamp specimens are shown in **Figure 7**.

DOI: https://doi.org/10.17509/ijost.v11i2.89779
p- ISSN 2528-1410 e- ISSN 2527-8045

Cement clay interlocking brick

Cement clay interlocking brick wall

CB1 aggregates

CB2 aggregates

**Figure 3.** Waste aggregates used in this study.

**Figure 4.** Low-cost steel clamps used in this study.

DOI: https://doi.org/10.17509/ijost.v11i2.89779
p- ISSN 2528-1410 e- ISSN 2527-8045

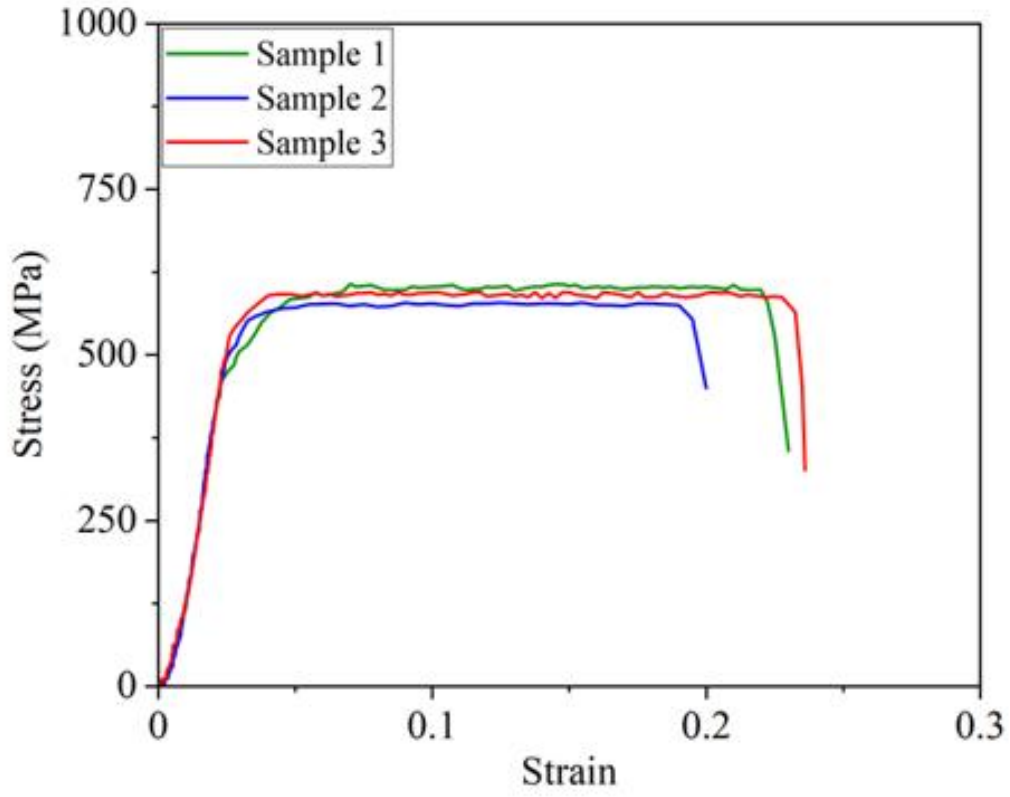


**Figure 5.** (a) tensile stress vs. strain response of three clamps, and (b) typical fracture observed during tensile testing.

**Figure 6.** Construction of specimens.

DOI: https://doi.org/10.17509/ijost.v11i2.89779
p- ISSN 2528-1410 e- ISSN 2527-8045

**Figure 7.** Typical low-cost steel clamp confined specimens.

### 2.4. Test Setup and Instrumentation

Compressive loading was employed utilizing a Universal Testing Machine (UTM). Prior to testing, steel plates were attached to both ends of each specimen to guarantee uniform load distribution. The reduction in specimen height during loading was measured using Linear Variable Differential Transformers, as illustrated in **Figure 8**. Axial strain corresponding to each load increment was estimated based on the recorded height reduction of the specimens.

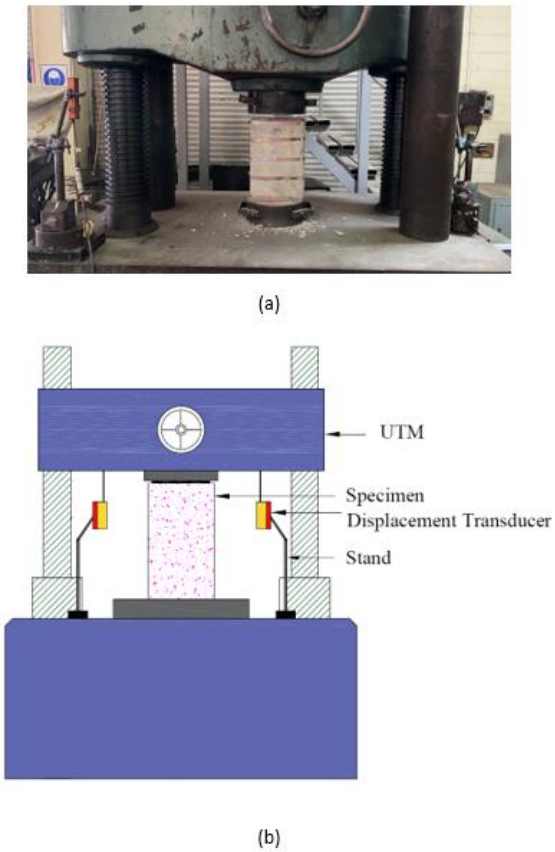


**Figure 8.** Test setup illustration, (a) lab view, (b) schematic.

DOI: https://doi.org/10.17509/ijost.v11i2.89779
p- ISSN 2528-1410 e- ISSN 2527-8045

## 3. RESULTS AND DISCUSSION

### 3.1. Observed Failure of Specimens

**Figure 9** illustrates the observed failure mechanisms across all test specimens. For better visualization, failure modes are compared within each group based on the level of confinement provided. In the control specimens, failure was primarily governed by splitting and crushing. Crushing was most evident near the loading zone, while splitting cracks extended along the specimen's length. Strengthened specimens displayed a uniform failure response under loading. Initially, no noticeable surface cracks appeared before the specimens reached their peak load. However, once peak capacity was exceeded, localized bulging developed in concrete areas not directly strengthened by the steel clamps. This bulging was ascribed to axial compressive stresses transferred through the steel clamps. During the load application, the core concrete continued efficiently confined by the clamps until clamp fracture occurred. Similar failure characteristics have also been reported in studies involving steel batten confinement systems [55,60]. In specimens with three steel clamps, lateral protruding of the concrete was minimal. Failure of the steel clamps typically occurred at or near the screw connections, and concrete crushing was primarily concentrated in the upper half of the specimen. With five clamps, more pronounced and evenly distributed bulging was observed, indicating improved confinement performance compared to the three-clamp setup. Specimens reinforced with eleven clamps showed the most effective confinement, as evidenced by extensive crushing and splitting patterns. These results imply that the eleven-clamp configuration provided superior resistance to both crushing and out-of-plane protruding. Notably, many of the upper clamps failed ascribed to the stress concentration. Similar failure modes in concrete cylinders subjected to steel clamp confinement, further supporting these findings [54].


**Figure 9.** Images taken at failure of specimens.

### 3.2. Compressive Response of Specimens

**Figure 10** presents the stress–strain behavior recorded for all tested specimens, categorized by their respective unconfined concrete strengths for clarity. The stress–strain curves can be idealized into two distinct segments: (1) an initial ascending branch leading up to the maximum stress (denoted as the peak strength), and (2) a descending straight branch

DOI: https://doi.org/10.17509/ijost.v11i2.89779
p- ISSN 2528-1410 e- ISSN 2527-8045

representing the post-peak degradation. A comparable trend was also observed in previous research on circular specimens confined using steel clamps, as documented [54], and square specimens, tested by [55]. Across all confinement groups, a clear improvement in peak strength was evident. However, the stiffness of the post-peak segment, designated as Z, was more gradual related to that of the corresponding unconfined specimens. The elastic modulus, representing the stiffness of the concrete before peak stress, remained unchanged between confined and reference samples within all groups. This suggests that the steel clamps functioned as passive confinement elements, activating only once the concrete exhibited significant lateral expansion. Since lateral dilation is closely linked to the level of axial compressive strain in the concrete core [60], the steel clamps had minimal effect at low strain levels. Furthermore, the strain at which peak strength occurred varied across the different groups, indicating that confinement influenced not only strength but also deformation characteristics. Detailed quantitative analysis of these parameters is presented in the following sections. An idealized response is also shown in **Figure 10(e)**. It is noted that several key points need to be approximated if the complete compressive behavior of confined concrete is desired. These include the peak strength $f_{cc}$, the corresponding strain $\epsilon_{cc}$, the elastic modulus $E_c$, and the slope of post-peak strength degradation branch $Z$. In this work, separate equations for these parameters are proposed in Section 4.

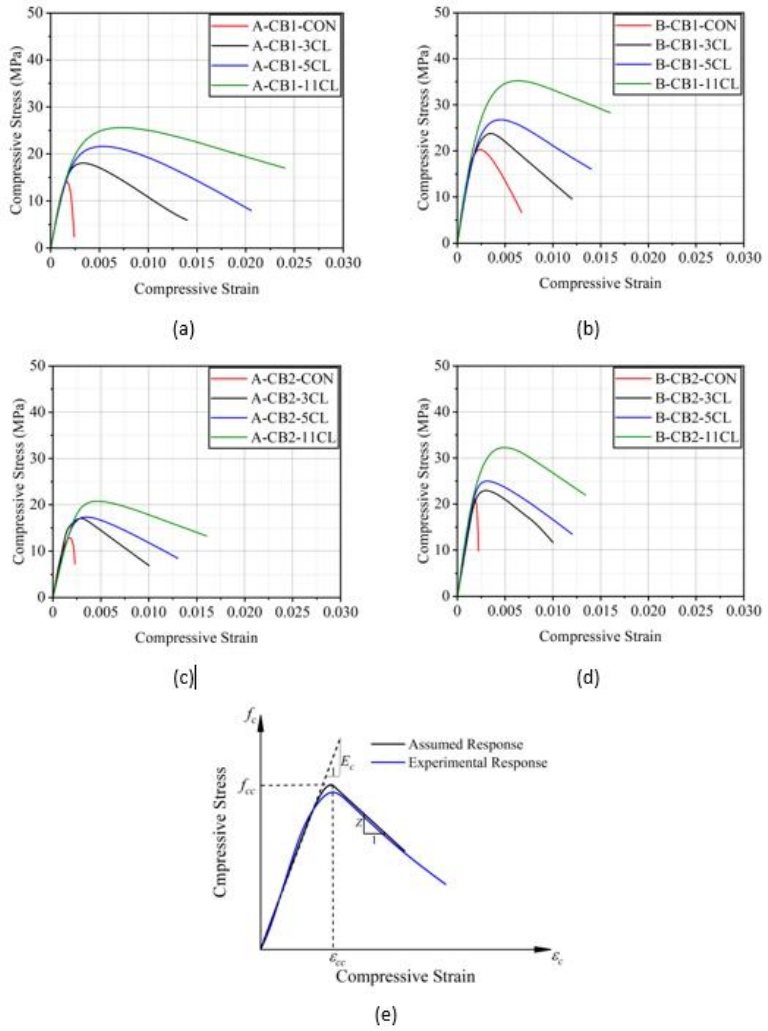


**Figure 10.** Measured response of specimens made with (a) low strength and CB1 bricks, (b) high strength and CB1 bricks, (c) low strength and CB2 bricks, (d) high strength and CB2 bricks, and (e) idealization of the typical response.

DOI: https://doi.org/10.17509/ijost.v11i2.89779
p- ISSN 2528-1410 e- ISSN 2527-8045

### 3.3. Summary of The Peak Compressive Strength and The Related Strain

**Table 4** summarizes the average values of peak strength and the corresponding strain at peak strength for each specimen group. These values represent the mean response of all samples within a given category. Significant improvements were recorded across all groups. The results indicate that enhancement in strength and strain was not uniform across the groups. In particular, subgroup G1A exhibited notable increases, with peak strength and strain at peak strength rising by up to 91.19% and 150.0%, respectively. It is important to note that this improvement varied across different subgroups, highlighting that the unconfined compressive strength and the type of recycled brick aggregates are important in determining the effectiveness of steel clamps confinement. Considering this, the following sections break down the effects of both these parameters on steel clamps confinement quantitatively.

**Table 4.** Summary of key parameters observed.

| Name | $f_{cc}$ (MPa) | Increase in $f_{cc}$ (%) | $\epsilon_{cc}$ | Increase in $\epsilon_{cc}$ (%) |
|---|---|---|---|---|
| A-CB1-CON | 15.10 | - | 0.0020 | - |
| A-CB1-3CL | 20.40 | 35.10 | 0.0033 | 65.00 |
| A-CB1-5CL | 23.20 | 53.64 | 0.0037 | 85.00 |
| A-CB1-11CL | 28.87 | 91.19 | 0.0050 | 150.00 |
| B-CB1-CON | 24.40 | - | 0.0019 | - |
| B-CB1-3CL | 25.69 | 5.29 | 0.0030 | 50.00 |
| B-CB1-5CL | 30.26 | 24.02 | 0.0035 | 75.00 |
| B-CB1-11CL | 38.00 | 55.74 | 0.0041 | 105.00 |
| A-CB2-CON | 14.92 | - | 0.0020 | - |
| A-CB2-3CL | 15.20 | 1.88 | 0.0028 | 40.00 |
| A-CB2-5CL | 18.80 | 26.01 | 0.0034 | 70.00 |
| A-CB2-11CL | 22.40 | 50.13 | 0.0040 | 100.00 |
| B-CB2-CON | 25.50 | - | 0.0018 | - |
| B-CB2-3CL | 26.00 | 1.96 | 0.0022 | 10.00 |
| B-CB2-5CL | 27.50 | 7.84 | 0.0027 | 35.00 |
| B-CB2-11CL | 33.00 | 29.41 | 0.0035 | 75.00 |

Note: $f_{cc}$ and $\epsilon_{cc}$ represent the peak compressive strength and the corresponding compressive strain, respectively.

### 3.4. Impact of The Confinement Ratio

The confinement ratio, referred to as the ratio of lateral confinement pressure $f_l$ to the compressive strength of unstrengthened concrete $f_{co}$, is a key parameter used to assess the effectiveness of external confinement systems [61,62]. This ratio helps establish a relation between the level of applied confinement and the resulting improvements in the axial compressive behavior of concrete. As reported in the literature, an increase in confinement ratio leads to greater axial strain for a given level of lateral strain [63]. In this work, the confinement pressure was estimated using a methodology analogous to that given by [64]. However, since the original formulation by [64] is specifically intended for reinforced concrete, it was adapted to be relevant for plain concrete elements. It is widely acknowledged that confinement in rectangular or square cross-sections is less effective than in circular sections [65]. To account for this, a horizontal confinement efficiency factor, $k_h$, is presented, as illustrated in **Figure 11(a)**. Additionally, vertical discontinuities between successive confinement layers, such as internal hoops [64], external steel confinement [66,67], or FRP battens [68,69], lead to further reductions in confinement effectiveness. This phenomenon is addressed using a vertical efficiency factor, $k_v$, depicted in **Figure 12(b)**. At the planar level,

DOI: https://doi.org/10.17509/ijost.v11i2.89779
p- ISSN 2528-1410 e- ISSN 2527-8045

it is assumed that the ineffectively confined zones develop outside a 45° parabolic boundary from each corner. The area beyond this boundary is considered ineffectively confined and is approximated mathematically as $(d-R_c)^2/6$ or $(b-R_c)^2/6$, where *b* and *d* are the cross-sectional dimensions and $R_c$ is the radius at corners. The complete area of ineffective confinement planar to steel clamps, denoted as $A_{ich}$, is calculated using Equation (1).

$$A_{ich} = \frac{(d-R_c)^2}{3} + \frac{(b-R_c)^2}{3} \quad (1)$$

By the subtraction of $A_{ich}$ from the gross area $A_g$, the planar area under effective confinement $A_{eh}$ may be deduced. Therefore, calculated using Equation (2).

$$A_{eh} = bd - \frac{(d-R_c)^2}{3} + \frac{(b-R_c)^2}{3} \quad (2)$$

The ratio of $A_{eh}$ to $A_g$ results in the horizontal confinement efficiency factor $k_h$, stated in Equation (3).

$$k_h = \frac{A_{eh}}{A_g} = \frac{\left[bd - \frac{(d-R_c)^2+(b-R_c)^2}{3}\right]}{bd} \quad (3)$$

Since the steel clamp confinement is discontinuous along the height, it is essential to take into account the reduced effect of confinement between consecutive clamps. Following the recommendations by [64], the effectively confined area midway between consecutive clamps is defined in Equation (4).

$$A_{ev} = \left(b - \frac{s'}{2}\right)\left(d - \frac{s'}{2}\right) \quad (4)$$

where the clear distance between two clamps is denoted by $s'$. Analogous to $k_h$, the vertical confinement efficiency factor $k_v$ is written in Equation (5).

$$k_v = \frac{A_{ev}}{A_g} = \frac{\left(b-\frac{s'}{2}\right)\left(d-\frac{s'}{2}\right)}{bd} \quad (5)$$

The resulting confinement efficiency factor $k_e$ is the product of $k_h$ and $k_v$, as recommended by Mander et al. [71] in Equation (6).

$$k_e = k_v \times k_h = \frac{\left(b-\frac{s'}{2}\right)\left(d-\frac{s'}{2}\right)}{bd} \times \frac{\left[bd - \frac{(d-R_c)^2+(b-R_c)^2}{3}\right]}{bd} \quad (6)$$

It is noted that different confinement pressures exist in orthogonal directions of rectangular-shaped specimens [64]. The confinement pressures in two orthogonal directions (say *x* and *y*) may be written in Equations (7) and (8).

$$f_{lx} = \frac{2A_{sc}f_{ysc}}{bs} \quad (7)$$

$$f_{ly} = \frac{2A_{sc}f_{ysc}}{ds} \quad (8)$$

where equations (7) and (8) take into account the effects of clamps cross-sectional area $A_{sc}$ and yield strength $f_{ysc}$. The effective confinement pressures are obtained by multiplying Equations (9) and (10) with $k_e$.

$$f_{lex} = f_{lx} \times k_e \quad (9)$$

$$f_{ley} = f_{ly} \times k_e \quad (10)$$

An overall lateral equivalent pressure $f_{le}$ is thus obtained by taking a weighted average [77] in Equation (11).

$$f_{le} = \frac{f_{lex}b + f_{ley}d}{b+d} \quad (11)$$

The computed efficiency factor $k_e$ for specimens confined with 3, 5, and 11 steel clamps was 0.17, 0.21, and 0.26, respectively. These correspond to effective confinement pressures of 0.33 MPa, 0.63 MPa, and 1.57 MPa, respectively. In equations (7) and (8), the yield strength of the steel clamps is utilized under the assumption that the clamps yield prior to the specimen reaching its peak load. Once yielding occurs, the confinement pressure is

DOI: https://doi.org/10.17509/ijost.v11i2.89779
p- ISSN 2528-1410 e- ISSN 2527-8045

considered constant, in line with recommendations from previous studies [70]. Accordingly, the yield strength is applied in all confinement-related calculations for both the ascending and descending branches of the compressive stress–strain response. The resulting confinement ratios across all specimens range from 0.013 to 0.11.

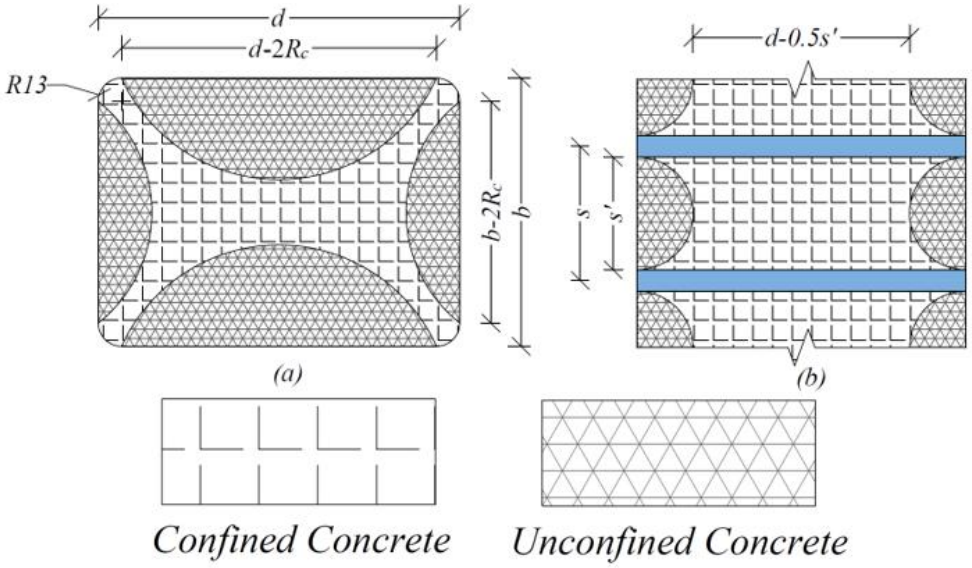


**Figure 11.** Visual representation of strengthened and unstrengthened areas at: (a) planar level and (b) along the height.

**Figures 12(a) and (b)** illustrate the variation in peak strength and strain at peak strength, respectively, for confined concrete made with different brick aggregates. The data reveal that the rate of improvement in both parameters differs depending on the type of aggregate used. Specifically, for a given confinement ratio, concrete incorporating CB1 aggregates exhibited the greatest enhancement. It is important to note that CB1 bricks generally possess higher compressive strength than CB2 bricks. These differences suggest that aggregate type significantly influences the confined behavior of concrete and should be incorporated into analytical models. Despite these variations, all aggregate types showed consistent gains in both peak strength and strain at peak strength with increasing confinement ratios, as depicted in **Figures 12(a) and 9(b)**.

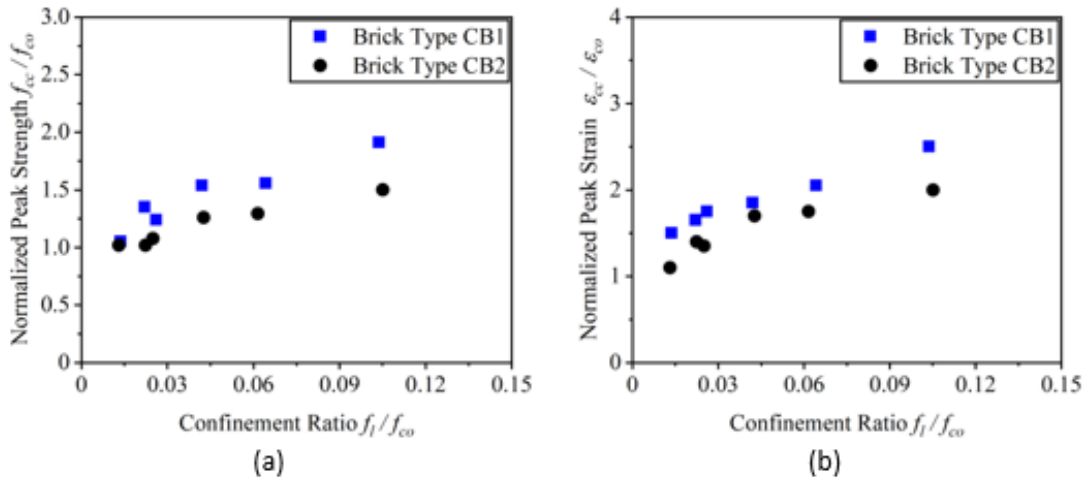


**Figure 12.** Effect of confinement ratio on: (a) $f_{cc}/f_{co}$ and (b) $\epsilon_{cc}/\epsilon_{co}$.

DOI: https://doi.org/10.17509/ijost.v11i2.89779
p- ISSN 2528-1410 e- ISSN 2527-8045

### 3.5. Modelling of Stress vs. Strain Compressive Response

To facilitate the practical application of the experimental findings, an analytical model was formulated to define the axial compressive stress vs. strain behavior of rectangular concrete specimens confined with steel clamps. This model is based on the widely recognized Popovics equation [71], presented in Equations (12) and (13), which is commonly utilized to characterize the compressive response of both confined and unconfined concrete. The objective of this modeling approach is to offer a straightforward and reliable method for predicting the stress–strain performance of steel clamp-confined concrete, using calibration from the present experimental findings.

$$f_c = f_{cc}\left[\frac{k\left(\frac{\epsilon_c}{\epsilon_{cc}}\right)}{k-1+\left(\frac{\epsilon_c}{\epsilon_{cc}}\right)^k}\right] \quad for\ \epsilon_c \le \epsilon_{cc} \tag{12}$$

$$k = \frac{E_c}{E_c - \frac{f_{cc}}{\epsilon_{cc}}} \tag{13}$$

In this method, the rising portion of the stress–strain curve is captured using a nonlinear expression introduced by Popovics, as shown in Equation (12). The shape-controlling parameter (k) is determined through Equation (13), which integrates the elastic modulus $E_c$, peak compressive strength $f_{cc}$, and the corresponding peak strain $\epsilon_{cc}$. **Figure 7(e)** provides a schematic representation of both the modeled and experimental stress–strain responses, highlighting essential parameters including the post-peak modulus *Z*.

#### 3.4.1. Regression based expression for $f_{cc}$

An empirical model was formulated through regression analysis of the experimental data to estimate the normalized peak compressive strength of rectangular concrete specimens confined with steel clamps, as a function of the confinement pressure $f_l$ and a normalized value of brick compressive strength $f_{bc}$. This is because both these parameters showed significant impact on $f_{cc}$, as noted in Section 3. The resulting predictive equation is presented in Equation (14).

$$\frac{f_{cc}}{f_{co}} = 1 + a \times \left(\frac{f_l}{f_{co}}\right)^b + c \times \left(\frac{f_{bc}}{f_{co}}\right)^d \tag{14}$$

where Gauss-Newton based nonlinear regression returned the values of 6.106, 1.027, $1.136\times10^{11}$, and 30.574 for *a*, *b*, *c*, and *d*, respectively. The coefficient of determination, i.e., $R^2$, was approximated to be 0.94, as shown graphically in **Figure 13(a)**.

#### 3.4.2. Regression based expression for $\epsilon_{cc}$

Analogous to $f_{cc}$, the strain at $f_{cc}$ was also dependent on the confinement pressure $f_l$ and a normalized value of brick compressive strength $f_{bc}$, as observed in Section 3. Thus, taking into account these independent variables, Equation (15) is proposed based on nonlinear regression analysis.

$$\frac{\epsilon_{cc}}{\epsilon_{co}} = 1 + a \times \left(\frac{f_l}{f_{co}}\right)^b + c \times \left(\frac{f_{bc}}{f_{co}}\right)^d \tag{15}$$

Using Gauss-Newton-based nonlinear regression, the parameters *a*, *b*, *c*, and *d*, were determined to be 4.592, 0.601, $8.560\times10^{10}$, and 30.413, respectively. The model demonstrated a strong fit with the experimental data, achieving a coefficient of determination $R^2$ of approximately 0.88, as illustrated in **Figure 13(b)**.

DOI: https://doi.org/10.17509/ijost.v11i2.89779
p- ISSN 2528-1410 e- ISSN 2527-8045

### 3.4.3. Regression based expression for $Z$

For the post-peak modulus Z, Equation (16) is proposed after several trials on different forms of nonlinear regression. Again, the independent variables were chosen to be the normalized brick compressive strength and the confinement ratio.

$$Z = a \times \left[ f_{co} + \frac{f_{co}}{\left(\frac{f_l}{f_{co}}\right)^b \left(\frac{f_{bc}}{f_{co}}\right)^c} \right]^d \quad (16)$$

The Gauss-Newton-based nonlinear regression yielded values of -222.723, 95.408, -42.459, and 0.004 for the parameters *a*, *b*, *c*, and *d*, respectively. The model showed a good agreement with the experimental data, with an $R^2$ of approximately 0.96, as depicted in **Figure 10(c)**.

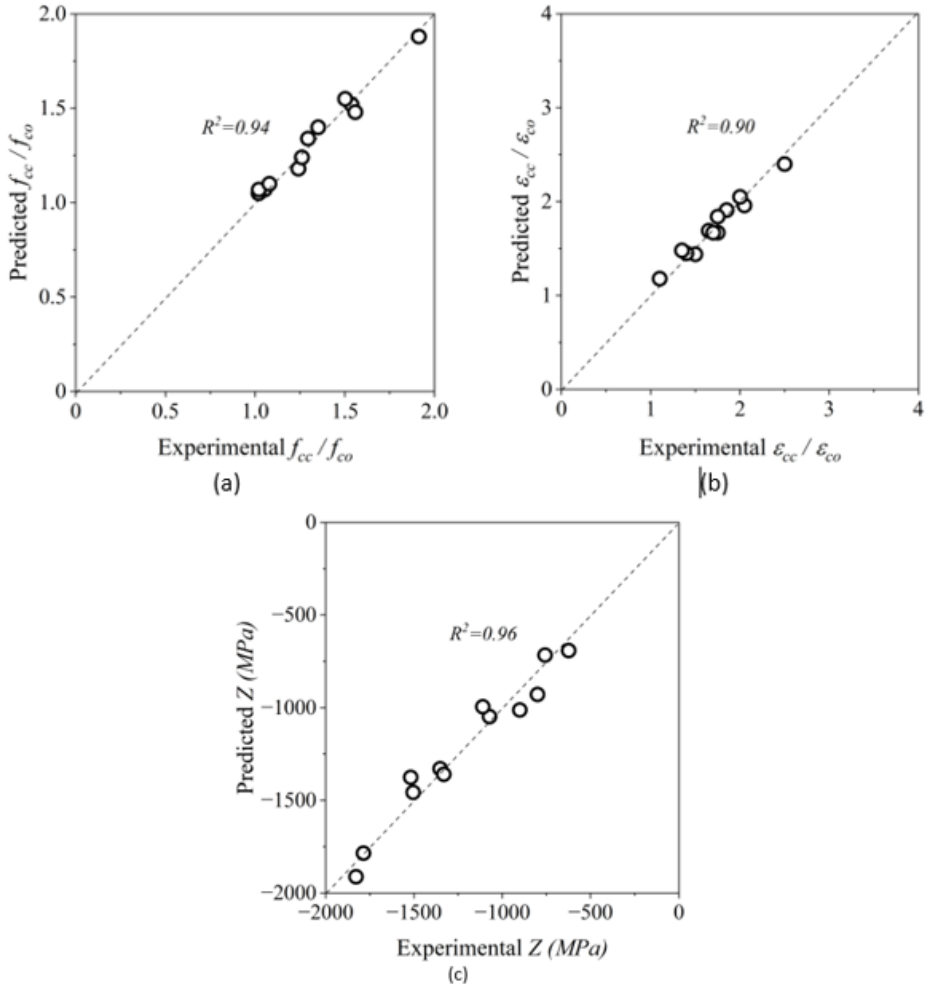


**Figure 13.** Agreement between the predicted and observed values for: (a) peak compressive strength, (b) strain at peak compressive strength, and (c) the post-peak modulus.

### 3.4.4. Agreement between predicted and observed response of steel clamp-confined concrete

To evaluate the reliability of the presented analytical expressions, the predicted stress vs. strain curves were evaluated against the experimental results for steel clamp-confined rectangular concrete specimens. These comparisons, categorized by concrete strength levels, A and B are shown in **Figure 14**. As illustrated in **Figure 14**, the predicted curves align closely

DOI: https://doi.org/10.17509/ijost.v11i2.89779
p- ISSN 2528-1410 e- ISSN 2527-8045

with the experimental data across all strength categories and confinement levels. For all groups, the models effectively reproduce both the ascending segment and the peak region of the stress–strain response. The post-peak behavior is also captured with reasonable accuracy, showing only slight discrepancies.

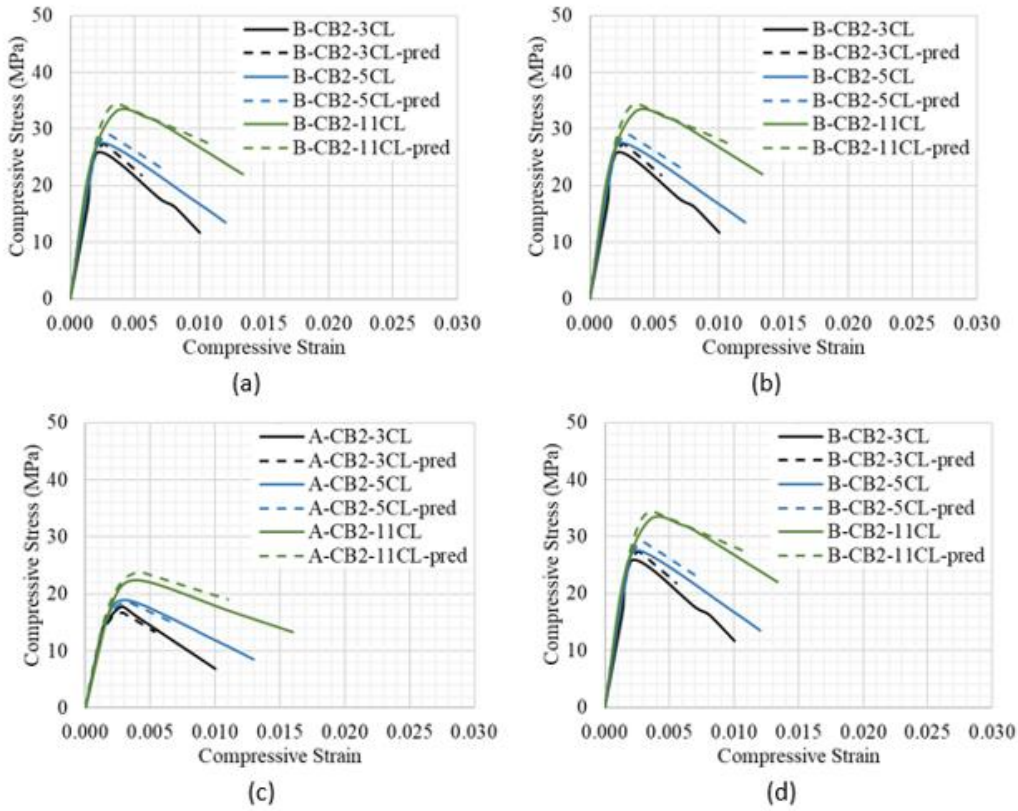


**Figure 14.** Agreement between observed and predicted response for specimens in subgroup: (a) G1A, (b) G1B, (c) G2A, and (d) G2B.

## 4. CONCLUSION

This study includes an experimental program involving monotonic compression tests on rectangular specimens confined with steel clamps. Key variables examined include the unconfined compressive strength of concrete, the number of steel clamps, and the type of coarse aggregates used. The following conclusions were derived from this work.

(i) The stress–strain response of all specimens exhibited a consistent two-phase behavior with clear improvements in peak strength due to confinement. Steel clamps provided passive confinement, activating only after significant lateral expansion, thus not affecting the initial stiffness. The post-peak slopes were more gradual in confined specimens, indicating enhanced ductility compared to unconfined counterparts. Variation in peak strain across groups highlights that confinement influenced both strength and deformation characteristics.

(ii) All groups showed substantial improvements, though the degree of enhancement varied, with up to 91.19% and 150.0% increases in strength and strain, respectively. These variations underscore the influence of unconfined compressive strength and the type of recycled brick aggregates on confinement effectiveness. Particularly, concrete made with brick aggregates of greater compressive strength showed better improvement in the compressive response.

DOI: https://doi.org/10.17509/ijost.v11i2.89779
p- ISSN 2528-1410 e- ISSN 2527-8045

(iii) Concrete made with CB1 aggregates demonstrated the most significant improvements at a given confinement ratio, likely due to their higher inherent compressive strength of bricks. These findings highlight the critical role of aggregate properties in confined concrete behavior and their relevance in model development. Nonetheless, all aggregate types exhibited consistent performance gains with increasing confinement, confirming the effectiveness of the strengthening technique.

(iv) Predictive models were established to estimate the peak strength, peak strain, and post-peak modulus of steel clamp-confined rectangular specimens. These models demonstrated strong accuracy, achieving $R^2$ values above 0.85, and were validated through comparison with experimental stress–strain data.

## 5. ACKNOWLEDGMENTS

This project is funded by National Research Council of Thailand (NRCT) and Thammasat University (Project Code: N42A670201). We also thanks to Asian Institute of Technology, Thailand for partially supporting testing facilities.

## 6. AUTHORS' NOTE

The authors declare that there is no conflict of interest regarding the publication of this article. The authors confirmed that the paper was free of plagiarism.

## 7. REFERENCES

[1] Tabsh, S. W., and Abdelfatah, A. S. (2009). Influence of recycled concrete aggregates on strength properties of concrete. *Construction and Building Materials*, *23*(2), 1163-1167.

[2] Prusty, J. K., and Patro, S. K. (2015). Properties of fresh and hardened concrete using agro-waste as partial replacement of coarse aggregate–A review. *Construction and Building Materials*, *82*, 101-113.

[3] Manjunath, B. A. (2016). Partial replacement of E-plastic waste as coarse-aggregate in concrete. *Procedia Environmental Sciences*, *35*, 731-739.

[4] Khatib, J. M. (2005). Properties of concrete incorporating fine recycled aggregate. *Cement and Concrete Research*, *35*(4), 763-769.

[5] Ren, F., Mo, J., Wang, Q., and Ho, J. C. M. (2022). Crumb rubber as partial replacement for fine aggregate in concrete: An overview. *Construction and Building Materials*, *343*, 128049.

[6] Dash, M. K., Patro, S. K., and Rath, A. K. (2016). Sustainable use of industrial-waste as partial replacement of fine aggregate for preparation of concrete–A review. *International Journal of Sustainable Built Environment*, *5*(2), 484-516.

[7] Xiong, Z., Wei, W., Liu, F., Cui, C., Li, L., Zou, R., and Zeng, Y. (2021). Bond behaviour of recycled aggregate concrete with basalt fibre-reinforced polymer bars. *Composite Structures*, *256*, 113078.

[8] Noguchi, T., Kitagaki, R., and Tsujino, M. (2011). Minimizing environmental impact and maximizing performance in concrete recycling. *Structural Concrete*, *12*(1), 36-46.

[9] Abdalla, T. A., Koteng, D. O., Shitote, S. M., and Matallah, M. (2022). Mechanical and durability properties of concrete incorporating silica fume and a high volume of sugarcane bagasse ash. *Results in Engineering*, *16*, 100666.

DOI: https://doi.org/10.17509/ijost.v11i2.89779
p- ISSN 2528-1410 e- ISSN 2527-8045

[10] Meng, T., Zhang, J., Wei, H., and Shen, J. (2020). Effect of nano-strengthening on the properties and microstructure of recycled concrete. *Nanotechnology Reviews*, *9*(1), 79-92.
[11] Zheng, C., Lou, C., Du, G., Li, X., Liu, Z., and Li, L. (2018). Mechanical properties of recycled concrete with demolished waste concrete aggregate and clay brick aggregate. *Results in Physics*, *9*, 1317-1322.
[12] Wang, D., Lu, C., Zhu, Z., Zhang, Z., Liu, S., Ji, Y., and Xing, Z. (2023). Mechanical performance of recycled aggregate concrete in green civil engineering. *Case Studies in Construction Materials*, *19*, e02384.
[13] Xiao, J., Li, W., Fan, Y., and Huang, X. (2012). An overview of study on recycled aggregate concrete in China (1996–2011). *Construction and Building Materials*, *31*, 364-383.
[14] Tam, V. W. (2008). Economic comparison of concrete recycling: A case study approach. *Resources, Conservation and Recycling*, *52*(5), 821-828.
[15] Silva, R. V., de Brito, J., and Dhir, R. K. (2014). Properties and composition of recycled aggregates from construction and demolition waste suitable for concrete production. *Construction and Building Materials*, *65*, 201-217.
[16] Meng, T., Yang, X., Wei, H., Meng, R., and Zhou, W. (2023). Study of the relationship between the water binder ratio and strength of mixed recycled aggregate concrete based on brick content. *Construction and Building Materials*, *394*, 132148.
[17] Liu, F., Liu, J., Ma, B., Huang, J., and Li, H. (2015). Basic properties of concrete incorporating recycled ceramic aggregate and ultra-fine sand. *Journal of Wuhan University of Technology-Material Science Education*, *30*(2), 352-360.
[18] Tanhadoust, A., Emadi, S. A. A., Nasrollahpour, S., Dabbaghi, F., and Nehdi, M. L. (2023). Optimal design of sustainable recycled rubber-filled concrete using life cycle assessment and multi-objective optimization. *Construction and Building Materials*, *402*, 132878.
[19] Ahmed, K. S., and Rana, L. R. (2023). Fresh and hardened properties of concrete containing recycled waste glass: A review. *Journal of Building Engineering*, *70*, 106327.
[20] Zhu, L., and Zhu, Z. (2020). Reuse of clay brick waste in mortar and concrete. *Advances in Materials Science and Engineering*, *2020*(1), 6326178.
[21] Li, H., Dong, L., Jiang, Z., Yang, X., and Yang, Z. (2016). Study on utilization of red brick waste powder in the production of cement-based red decorative plaster for walls. *Journal of Cleaner Production*, *133*, 1017-1026.
[22] Maaze, M. R., and Shrivastava, S. (2023). Design development of sustainable brick-waste geopolymer brick using full factorial design methodology. *Construction and Building Materials*, *370*, 130655.
[23] Martín-Morales, M., Zamorano, M., Ruiz-Moyano, A., and Valverde-Espinosa, I. (2011). Characterization of recycled aggregates construction and demolition waste for concrete production following the Spanish Structural Concrete Code EHE-08. *Construction and Building Materials*, *25*(2), 742-748.
[24] Thomas, C., Setién, J., and Polanco, J. A. (2016). Structural recycled aggregate concrete made with precast wastes. *Construction and Building Materials*, *114*, 536-546.
[25] Azunna, S. U., and Ogar, J. O. (2021). Characteristic properties of concrete with recycled burnt bricks as coarse aggregates replacement. *Computational Engineering and Physical Modeling*, *4*(1), 56-72.
[26] Ma, K., Huang, X., Shen, J., Hu, M., Long, G., Xie, Y., and Zhang, W. (2021). The morphological characteristics of brick-concrete recycled coarse aggregate based on the digital image processing technique. *Journal of Building Engineering*, *44*, 103292.

DOI: https://doi.org/10.17509/ijost.v11i2.89779
p- ISSN 2528-1410 e- ISSN 2527-8045

[27] Khoury, E., Ambrós, W., Cazacliu, B., Sampaio, C. H., and Remond, S. (2018). Heterogeneity of recycled concrete aggregates, an intrinsic variability. *Construction and Building Materials*, *175*, 705-713.

[28] Xiao, J. Z., Li, J. B., and Zhang, C. (2006). On relationships between the mechanical properties of recycled aggregate concrete: An overview. *Materials and Structures*, *39*(6), 655-664.

[29] Meng, T., Wei, H., Dai, D., Liao, J., AND Ahmed, S. (2022). Effect of brick aggregate on failure process of mixed recycled aggregate concrete via X-CT. *Construction and Building Materials*, *327*, 126934.

[30] Del Bosque, I. S., Zhu, W., Howind, T., Matías, A., De Rojas, M. S., and Medina, C. (2017). Properties of interfacial transition zones (ITZs) in concrete containing recycled mixed aggregate. *Cement and Concrete Composites*, *81*, 25-34.

[31] Yue, G., Ma, Z., Liu, M., Liang, C., and Ba, G. (2020). Damage behavior of the multiple ITZs in recycled aggregate concrete subjected to aggressive ion environment. *Construction and Building Materials*, *245*, 118419.

[32] Aliabdo, A. A., Abd-Elmoaty, A. E. M., and Hassan, H. H. (2014). Utilization of crushed clay brick in concrete industry. *Alexandria Engineering Journal*, *53*(1), 151-168.

[33] Sri Ravindrarajah, R., and Tam, C. T. (1985). Properties of concrete made with crushed concrete as coarse aggregate. *Magazine of Concrete Research*, *37*(130), 29-38.

[34] Debieb, F., and Kenai, S. (2008). The use of coarse and fine crushed bricks as aggregate in concrete. *Construction and Building Materials*, *22*(5), 886-893.

[35] Cachim, P. B. (2009). Mechanical properties of brick aggregate concrete. *Construction and Building Materials*, *23*(3), 1292-1297.

[36] Poon, C. S., Shui, Z. H., Lam, L., Fok, H., and Kou, S. C. (2004). Influence of moisture states of natural and recycled aggregates on the slump and compressive strength of concrete. *Cement and Concrete Research*, *34*(1), 31-36.

[37] Uddin, M. T., Mahmood, A. H., Kamal, M. R. I., Yashin, S. M., and Zihan, Z. U. A. (2017). Effects of maximum size of brick aggregate on properties of concrete. *Construction and Building Materials*, *134*, 713-726.

[38] Wang, T., Cui, S., Ren, X., Zhang, W., Yang, X., Gong, S., and Yu, X. (2024). Study on the mechanical properties and microstructure of recycled brick aggregate concrete with waste fiber. *Reviews on Advanced Materials Science*, *63*(1), 20230175.

[39] Khalaf, F. M., and DeVenny, A. S. (2004). Recycling of demolished masonry rubble as coarse aggregate in concrete. *Journal of Materials in Civil Engineering*, *16*(4), 331-340.

[40] Tanta, A., Kanoungo, A., Singh, S., and Kanoungo, S. (2022). The effects of surface treatment methods on properties of recycled concrete aggregates. *Materials Today: Proceedings*, *50*, 1848-1852.

[41] Tam, V. W., and Tam, C. M. (2007). Assessment of durability of recycled aggregate concrete produced by two-stage mixing approach. *Journal of Materials Science*, *42*(10), 3592-3602.

[42] Yang, J., Du, Q., and Bao, Y. (2011). Concrete with recycled concrete aggregate and crushed clay bricks. *Construction and Building Materials*, *25*(4), 1935-1945.

[43] Yuan, S., Li, K., Luo, J., Zhu, Z., Zeng, Y., Dong, J., and Zhang, F. (2023). Effects of brick-concrete aggregates on the mechanical properties of basalt fiber reinforced recycled waste concrete. *Journal of Building Engineering*, *80*, 108023.

[44] Gao, D., Jing, J., Chen, G., and Yang, L. (2019). Experimental investigation on flexural behavior of hybrid fibers reinforced recycled brick aggregates concrete. *Construction and building materials*, *227*, 116652.

DOI: https://doi.org/10.17509/ijost.v11i2.89779
p- ISSN 2528-1410 e- ISSN 2527-8045

[45] Choudhury, M. S. I., Amin, A. F. M. S., Islam, M. M., and Hasnat, A. (2016). Effect of confining pressure distribution on the dilation behavior in FRP-confined plain concrete columns using stone, brick and recycled aggregates. *Construction and Building Materials*, *102*, 541-551.

[46] Jiang, T., Wang, X. M., Zhang, W. P., Chen, G. M., and Lin, Z. H. (2020). Behavior of FRP-confined recycled brick aggregate concrete under monotonic compression. *Journal of Composites for Construction*, *24*(6), 04020067.

[47] Gao, C., Huang, L., Yan, L., Kasal, B., and Li, W. (2016). Behavior of glass and carbon FRP tube encased recycled aggregate concrete with recycled clay brick aggregate. *Composite structures*, *155*, 245-254.

[48] Mi, T., Peng, L., Yu, K., and Zhao, Y. (2023). Enhancement strategies for recycled brick aggregate concrete using MICP and EICP treatments. *Journal of Building Engineering*, *79*, 107909.

[49] Manzur, T., Huq, R. S., Efaz, I. H., Afroz, S., Rahman, F., AND Hossain, K. (2019). Performance enhancement of brick aggregate concrete using microbiologically induced calcite precipitation. *Case Studies in Construction Materials*, *11*, e00248.

[50] Wang, W., Wang, S., Peng, L., Wang, N., Meng, T., Zhao, Y., and Gong, F. (2024). Preliminary investigation and life cycle assessment of artificial reefs with recycled brick-concrete aggregates. *Construction and Building Materials*, *432*, 136618.

[51] Yooprasertchai, E., Dithaem, R., Arnamwong, T., Sahamitmongkol, R., Jadekittichoke, J., Joyklad, P., and Hussain, Q. (2021). Remediation of punching shear failure using glass fiber reinforced polymer (Gfrp) rods. *Polymers*, *13*(14), 2369.

[52] Iskander, M. G., and Hassan, M. (1998). State of the practice review in FRP composite piling. *Journal of Composites for Construction*, *2*(3), 116-120.

[53] Munir, M. J., Kazmi, S. M. S., Wu, Y. F., and Lin, X. (2021). Axial stress-strain performance of steel spiral confined acetic acid immersed and mechanically rubbed recycled aggregate concrete. *Journal of Building Engineering*, *34*, 101891.

[54] Rodsin, K., Joyklad, P., Hussain, Q., Mohamad, H., Buatik, A., Zhou, M., and Elnemr, A. (2022). Behavior of steel clamp confined brick aggregate concrete circular columns subjected to axial compression. *Case Studies in Construction Materials*, *16*, e00815.

[55] Ejaz, A., Ruangrassamee, A., Jirawattanasomkul, T., and Zhang, D. (2025). Experimental and analytical investigations on enhancing compressive stress vs. strain response of square-section recycled brick aggregate concrete by steel clamps. *Case Studies in Construction Materials*, *22*, e04645.

[56] Thansirichaisree, P., Mohamad, H., Ejaz, A., Saingam, P., Hussain, Q., and Suparp, S. (2024). Stress-strain behavior of square concrete columns confined with hybrid B-CSM composites and development of novel prediction models. *Composites Part C: Open Access*, *14*, 100448.

[57] Hussain, Q., Ruangrassamee, A., Jirawattanasomkul, T., and Zhang, D. (2024). Stress and strain relations of RC circular, square and rectangular columns externally wrapped with fiber ropes. *Scientific Reports*, *14*(1), 4181.

[58] Wang, W., Sheikh, M. N., and Hadi, M. N. (2016). Axial compressive behaviour of concrete confined with polymer grid. *Materials and Structures*, *49*(9), 3893-3908.

[59] Ozbakkaloglu, T., and Fanggi, B. L. (2014). Axial compressive behavior of FRP-concrete-steel double-skin tubular columns made of normal-and high-strength concrete. *Journal of Composites for Construction*, *18*(1), 04013027.

[60] Rong, C., and Shi, Q. (2020). Behaviour of angle steel frame confined concrete columns under axial compression. *Construction and Building Materials*, *241*, 118034.

DOI: https://doi.org/10.17509/ijost.v11i2.89779
p- ISSN 2528-1410 e- ISSN 2527-8045

[61] Li, P. D., Zeng, Q., Gao, S. J., and Yuan, F. (2024). Postpeak stress–strain behavior of high-strength concrete under different FRP confinement stiffness ratios. *Journal of Composites for Construction*, *28*(2), 04024003.

[62] Vu, X. H., Malecot, Y., Daudeville, L., and Buzaud, E. (2009). Experimental analysis of concrete behavior under high confinement: Effect of the saturation ratio. *International Journal of Solids and Structures*, *46*(5), 1105-1120.

[63] Teng, J. G., Huang, Y. L., Lam, L., and Ye, L. P. (2007). Theoretical model for fiber-reinforced polymer-confined concrete. *Journal of Composites for Construction*, *11*(2), 201-210.

[64] Mander, J. B., Priestley, M. J. N., and Park, R. (1988). Observed stress-strain behavior of confined concrete. *Journal of Structural Engineering*, *114*(8), 1827-1849.

[65] Mostofinejad, D., Moshiri, N., and Mortazavi, N. (2015). Effect of corner radius and aspect ratio on compressive behavior of rectangular concrete columns confined with CFRP. *Materials and Structures*, *48*(1), 107-122.

[66] Rong, C., and Shi, Q. (2020). Behaviour of angle steel frame confined concrete columns under axial compression. *Construction and Building Materials*, *241*, 118034.

[67] Shhatha, M. A., Mahdi, W. H., and Alalikhan, A. A. (2023). Assessment for behavior of axially loaded reinforced concrete columns strengthened by different patterns of steel-framed jacket. *Open Engineering*, *13*(1), 20220414.

[68] Saljoughian, A., and Mostofinejad, D. (2016). Corner strip-batten technique for FRP-confinement of square RC columns under eccentric loading. *Journal of Composites for Construction*, *20*(3), 04015077.

[69] Mostofinejad, D., and Ilia, E. (2014). Confining of square RC columns with FRP sheets using corner strip–batten technique. *Construction and Building Materials*, *70*, 269-278.

[70] Harries, K. A., and Kharel, G. (2003). Experimental investigation of the behavior of variably confined concrete. *Cement and Concrete research*, *33*(6), 873-880.

[71] Popovics, S. (1973). A numerical approach to the complete stress-strain curve of concrete. *Cement and Concrete Research*, *3*(5), 583-599.

DOI: https://doi.org/10.17509/ijost.v11i2.89779
p- ISSN 2528-1410 e- ISSN 2527-8045